Magic Momenta and Three-Dimensional Landau Levels from a Three-Dimensional Graphite Moiré Superlattice

Xin Lu,[1,2,*] Bo Xie,[1,2,*] Yue Yang,[1,*] Yiwen Zhang,[1,2] Xiao Kong,[3,4] Jun Li,[1,2] Feng Ding,[3,5] Zhu-Jun Wang,[1,†] and Jianpeng Liu[1,2,6,‡]

[1]*School of Physical Science and Technology, ShanghaiTech University, Shanghai 201210, China*
[2]*ShanghaiTech Laboratory for Topological Physics, ShanghaiTech University, Shanghai 201210, China*
[3]*Institute of Technology for Carbon Neutrality, Shenzhen Institute of Advanced Technology, Chinese Academy of Sciences, Shenzhen, China*
[4]*Shanghai Institute of Microsystem and Information Technology, Chinese Academy of Sciences, Shanghai, China*
[5]*Faculty of Materials Science and Energy Engineering, Shenzhen University of Advanced Technology, Shenzhen, China*
[6]*Liaoning Academy of Materials, Shenyang 110167, China*

(Received 25 September 2023; revised 17 November 2023; accepted 4 January 2024; published 2 February 2024)

In this Letter, we theoretically explore the physical properties of a new type of *three-dimensional graphite moiré superlattice*, the bulk alternating twisted graphite (ATG) system with homogeneous twist angle, which is grown by *in situ* chemical vapor decomposition method. Compared to twisted bilayer graphene (TBG), the bulk ATG system is bestowed with an additional wave vector degree of freedom due to the extra dimensionality. As a result, when the twist angle of bulk ATG is smaller than twice of the magic angle of TBG, there always exist "magic momenta" which host topological flat bands with vanishing in-plane Fermi velocities. Most saliently, when the twist angle is relatively large, a dispersionless three-dimensional zeroth Landau level would emerge in the bulk ATG, which may give rise to robust three-dimensional quantum Hall effects and unusual quantum-Hall physics over a large range of twist angles.

DOI: 10.1103/PhysRevLett.132.056601

Twisted bilayer graphene (TBG) [1–3] has aroused significant interest in recent years. When the twist angle of TBG is around the "magic angles" [1], the lowest two bands per spin per valley become ultraflat, and even turn out to be exactly flat in the chiral limit [4]. These flat bands are further found to be topologically nontrivial with Landau-level like wave functions [4–12]. The unprecedented flatness combined with nontrivial band topology yields plentiful phenomena in magic-angle TBG such as superconductivity, correlated insulators, quantum anomalous Hall effect, orbital magnetic states, and so on [13–36], which have stimulated tremendous theoretical research [9,10,37–61].

It is well appreciated that tuning a TBG sample to the vicinity of the first magic angle ($\theta_m^{(1)} \approx 1.05°$) is extremely challenging, especially if the device were fabricated based on the traditional transferring and stacking technique [62,63]. Nevertheless, the stringent magic-angle condition for the emergence of flat bands in TBG can be somehow released by stacking more twisted graphene layers in the out-of-plane direction, forming twisted multilayer graphene (TMG) [64–72] and alternating twisted multilayer graphene (ATMG) [73–77] systems, where topological flat bands are robustly present over a finite range of twist angles or at larger values of magic angles. Various exotic states such as unconventional superconductivity [78,79], quantum anomalous Hall effect [80], and generalized Wigner crystals [81] etc., have been observed in these TMG and ATMG systems. From the perspective of fundamental science, it is then natural to ask what kind of new states and new phenomena would emerge when an infinite number of layers of twisted graphene are stacked on top of each other, forming a three-dimensional graphite moiré superlattice.

Recently, an origami-kirigami approach by chemical vapor deposition (CVD) growth has been developed for the fabrication of graphene spiral [82]. Using such a technique, double-helix structure of hundreds of interwinded graphene layers with uniform interlayer twist angle has been successfully achieved [see Fig. 1(a) and Supplemental Material, video 1 [83]]. The top view of the dual-helical graphene spiral [top panel of Fig. 1(b)] indicates a periodic superlattice arrangement. Away from the central dislocation line, the system exhibits an alternating twisted pattern between each of the two adjacent graphene layers, wherein intraplane moiré superlattice vectors [$\mathbf{t}_1$, $\mathbf{t}_2$ in the top panel of Fig. 1(b)] can be identified. In principle, it is feasible to achieve the growth of infinite graphene layers along the vertical screw dislocation, which for the first time realizes a genuine three-dimensional moiré graphite superlattice with alternating interlayer twist angle. In Fig. 1(c), the transmission electron microscopy (TEM) image of the twisted graphene spiral sample is presented. Employing mask filtering and inverse

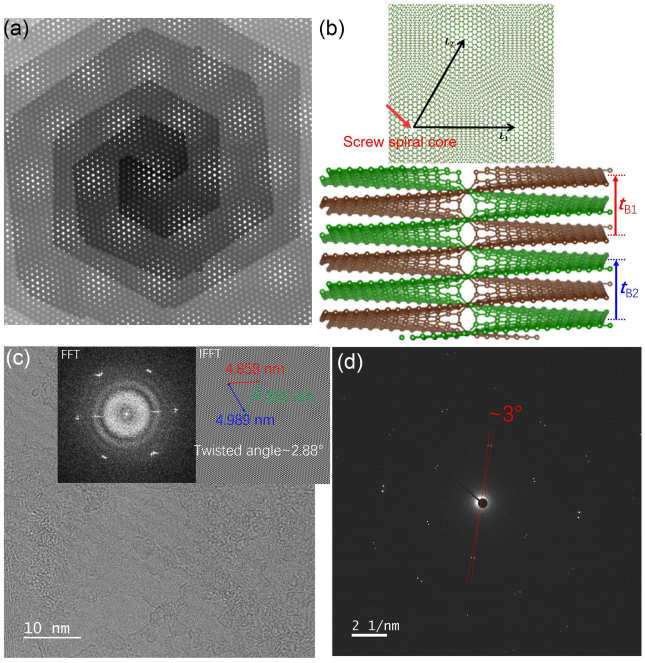

FIG. 1. Structural characterizations of bulk alternating twisted graphite. (a) The structural model of a graphene spiral with alternating interlayer twist angle. (b) The top view and the cross-sectional illustration ($\mathbf{t}_{B1}$ and $\mathbf{t}_{B2}$ denote Burgers vectors) of the structural model. (c) High-resolution TEM image of the twisted spiral graphene sample. (d) Electron diffraction pattern.

fast Fourier transform processing in digital micrograph, the TEM image distinctly demonstrates a moiré pattern characterized by an average superlattice constant of $L_s = a/[2\sin(\theta/2)] = 4.9$ nm [inset of Fig. 1(c), $a = 2.46$ Å is graphene's lattice constant], corresponding to a twist angle $\theta \approx 2.9°$. As depicted in Fig. 1(d), the electron diffraction patterns from two sets of twisted graphene layers are clearly distinguishable, yielding a measured twist angle of approximately 3°, in concordance with the deduction from the real-space moiré superlattice constant. The cross-sectional scanning transmission electron microscopy (STEM) image offers a contrasting feature of the double-helix graphene spiral, which confirms the successful growth of two sets of alternatingly twisted graphene layers following the helical dislocation path [83]. All these structural characterizations are also presented in the Supplemental Material, video 2 [83]. A noteworthy observation is that this screw dislocation itself hosts bound states [83]. The successful realization of this macroscopically extensive bulk alternating twisted graphite (ATG) system effectively extends the realm of intriguing moiré graphene superlattices physics from two dimensions to three dimensions.

In this Letter, we theoretically study the electronic structures, topological properties, and Landau levels (LLs) of the bulk ATG system. The additional dimensionality endows bulk ATG an additional wave vector degree of freedom to explore flat-band physics of magic-angle TBG. In particular, we find that when the twist angle $\theta \leq 2\theta_m^{(1)} \approx 2.1°$, one can always find a "magic quasi momentum" $\hbar k_z^*$ at which the 2D band structures and wave functions within the k_x-k_y plane are exactly the same as those of TBG at the first magic angle. Moreover, when the twist angle θ is smaller than twice of the nth magic angle $\theta_m^{(n)}$ (with $n = 2, 3, \ldots$), then for each θ, there are at least n magic momenta $\{k_z^{(s),*}, s = 1, \ldots, n\}$ at which the band structures and wave functions within the k_x-k_y planes are exactly the same as those of TBG at the sth magic angle $\theta_m^{(s)}$. In other words, when $\theta \leq \theta_m^{(2)} \approx 1°$, multiple flat bands with distinct topological properties would coexist in the same bulk ATG system. For larger twist angles $\theta > 2\theta_m^{(1)} \approx 2.1°$, Dirac-cone type band structures with finite Fermi velocities persist for every k_z in the Brillouin zone. The Dirac points are almost perfectly aligned on a chain in the k_z direction, leading to weakly dispersive *three-dimensional LLs*. Most saliently, given that the zeroth LL of graphene is exactly pinned to the Dirac point, there exists a branch of *dispersionless zeroth 3D Landau band* emerging from bulk ATG under vertical magnetic fields, which may give rise to robust 3D quantum Hall effects (QHE) at its full filling.

Magic momenta.—Neglecting the spiral dislocation at the core, we can consider bulk ATG as an infinite aligned stacking of TBG in the out-of-plane direction with lattice constant $2d_0 = 6.7$ Å. The coupling between two nearest neighbor TBG motifs is just the first-neighbor interlayer moiré potential. Such a picture leads straight to a low-energy effective Hamiltonian for bulk ATG [83] based on the continuum model [1,2,97] of TBG with twist angle θ:

$$\mathrm{H}_\theta^\mu = \begin{bmatrix} -\hbar v_F(\mathbf{k} - \mathbf{K}_1^\mu)\cdot\boldsymbol{\sigma}^\mu & T(1 + e^{i\phi}) \\ T^\dagger(1 + e^{-i\phi}) & -\hbar v_F(\mathbf{k} - \mathbf{K}_2^\mu)\cdot\boldsymbol{\sigma}^\mu \end{bmatrix}, \quad (1)$$

where the Fermi velocity is $\hbar v_F/a = 2.1354$ eV [84] with graphene's lattice constant $a = 2.46$ Å. Neglecting the intervalley coupling, the diagonal blocks represent the $\mathbf{k}\cdot\mathbf{p}$ Hamiltonian of the two layers of graphene in valley $\mu = \pm 1$ near the Dirac points $\mathbf{K}_{1/2}^\mu$ with the Pauli matrices $\boldsymbol{\sigma}^\mu = (\mu\sigma_x, \sigma_y)$ defined in the sublattice space, and $\mathbf{k} = (k_x, k_y)$. The off-diagonal term T [83] stands for the interlayer moiré potential. The phase factor $e^{\pm i\phi} = e^{\pm i2k_z d_0}$ is the only new contribution arising from the nearest neighbor interlayer couplings along the opposite out-of-plane directions in such 3D bulk system. Here, it is naturally expected that the distance between two adjacent graphene layers is fixed, denoted as d_0, since there is no space for out-of-plane corrugations in such a 3D moiré superlattice. This postulation is verified by direct molecular dynamics simulations of bulk ATG, which gives $d_0 = 3.35$ Å [83].

The moiré potential T are characterized by intra- and intersublattice interlayer tunnelling amplitudes $u_0 = u_0' = 0.103$ eV. Up to an overall bandwidth $\hbar v_F k_\theta$ [with $k_\theta = 4\pi/(3L_s)$], when $u_0 = u_0'$ the continuum model of

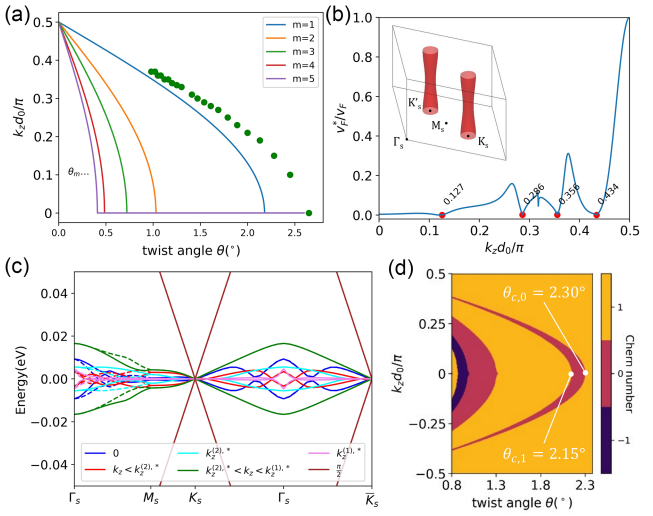

FIG. 2. (a) Evolution of magic momenta $k_z^{(m),*}$ as a function of twist angle θ. The green dots are the results from tight-binding calculations [83]. (b) Evolution of Fermi velocity near the moiré K point as a function of k_z for $\theta = 0.45°$. The red dots indicate the four magic momenta. Inset shows Fermi surface at $\theta = 7°$ with Fermi energy 0.1 eV. (c) Evolution of bulk ATG (with $\theta = 0.8°$) 2D band structures in the (k_x, k_y) plane from $k_z d_0 = 0$ to $\pi/2$, where $k_z^{(1),*}$ and $k_z^{(2),*}$ mark the two magic momenta. (d) Chern number of the valence flat band of bulk ATG in valley K as a function of k_z and θ.

TBG is fully characterized by a dimensionless ratio $\alpha_0(\theta) = u_0'/(\hbar v_F k_\theta)$. Similarly, since k_z is a good quantum number and the bulk ATG can be seen as a series of decoupled TBG indexed by k_z, the noninteracting physics of each of them is totally governed by

$$\alpha(k_z, \theta) = \alpha_0(\theta)|1 + e^{2ik_z d_0}|, \tag{2}$$

where $k_z d_0 \in [0, \pi]$. Therefore, given a twist angle θ, one can explore a range of k_z-dependent effective moiré potential, which varies from zero ($k_z = \pi/2d_0$) to doubled moiré potential strength ($k_z = 0$) of the corresponding isolated TBG. In the small-angle approximation, as long as $\theta/2$ is smaller than sth magic angle $\theta_m^{(s)}$ of TBG, one can always find the corresponding sth *magic momentum* $k_z^{(s),*}$ such that $\alpha(k_z^{(s),*}, \theta) = \alpha_0(\theta_m^{(s)})$, as shown in Fig. 2(a). For example, to achieve the flat bands at the first magic angle in TBG, it only suffices to twist the bulk ATG of angle $\theta < 2\theta_m^{(1)} \approx 2.1°$. Furthermore, the bulk ATG can simultaneously host flat bands of TBG at several magic angles if $\theta < 2\theta_m^{(n)}$ with $n \geq 2$. Accordingly, we can define n magic momenta $\{k_z^{(s),*}, s = 1, \ldots, n\}$ for bulk ATG at fixed twist angle $\theta < 2\theta_m^{(n)}$. For example, if $\theta = 0.45° < 2 \times \theta_m^{(4)}$, the flat bands of TBG from first to fourth magic angle emerge concomitantly in the bulk ATG at four magic momenta, as shown in Fig. 2(b). In Fig. 2(c), we present the moiré band structures of bulk ATG with $\theta = 0.8°$ at several different k_z. In such a case, $2\theta_m^{(3)} < \theta < 2\theta_m^{(2)}$, topological flat bands at the first and second magic angles of TBG coexist at different magnetic momenta $k_z^{(1),*}$ and $k_z^{(2),*}$, as plotted by cyan and magenta lines in Fig. 2(c). It is worth noting that in Ref. [73], Khalaf *et al.* argued the presence of "a continuum of magic angles" when $\theta < 2\theta_m^{(1)}$ in the inifinite-layer limit of ATMG. In the above discussions we have shown that the continuum of magic angles are manifested as θ-dependent magic momenta in the 3D bulk limit.

Band topology.—Since bulk ATG integrates a continuum of k_z-indexed TBG into a single bulk system, it is intriguing to explore the topological properties by varying both θ and k_z. By introducing a small sublattice mass term (∼0.1 meV) into the Hamiltonian Eq. (1), the Dirac points are gapped out such that every band can be associated with a Chern number. At each k_z and θ, we calculate the Chern number of the valence flat band from valley K, and the calculated topological phase diagram is shown in Fig. 2(d). First, the Chern number can change only if the twist angle of bulk ATG θ is smaller than $\theta_{c,0} = 2.3°$, which corresponds to the apex point of the rightmost phase boundary. From right to left across $\theta_{c,0}$, the Chern number at $k_z = 0$ switches from 1 to 0. Nevertheless, the Chern number shifts back to unity if θ is smaller than another critical angle $\theta_{c,1} = 2.15°$. If one continues to decrease θ, a series of such phase boundaries are passed, resulting in a rich topological phase diagram as shown in Fig. 2(d) [83].

3D quantum Hall effect.—The unusual band dispersions and nontrivial topological properties of bulk ATG imply its unconventional responses to electromagnetic fields. It follows from Eq. (1) that k_z plays a special role compared to the other two wave vectors, leading to a strongly anisotropic, quasi-2D Fermi surface as shown in the inset of Fig. 2(b), which is desirable to realize 3D QHE [98,99]. To this end, the twist angle of the bulk ATG should be sufficiently larger than $2\theta_m^{(1)}$, otherwise at some k_z the lowest bands would flatten, which suppresses LL spacing thus disfavors QHE. In the case of large twist angles, the moiré potential can be treated by perturbation theory, and the bulk ATG around each Dirac point can be described by a Dirac Hamiltonian with renormalized Fermi velocity

$$H_{\text{eff}} = \hbar v_F[1 - 9\alpha^2(k_z, \theta)](k_x \sigma_x + k_y \sigma_y), \tag{3}$$

which is valid if $\theta \gtrapprox 6°$ based on an attempting criterion $9\alpha^2(k_z, \theta) < 0.1$. In practice, 3D QHE is present at even smaller angles (numerically checked at least for $\theta \gtrapprox 4°$). Based on the Hamiltonian Eq. (3), at fixed k_z, the LL should be exactly the same as graphene but with k_z-dependent LL spacing. Remarkably, for every k_z there exists the zeroth LL exactly pinned at the Dirac point, which remains robust even in the presence of slight inhomogeneity and disorder by virtue of Atiyah-Singer index theorem [100]. This gives rise

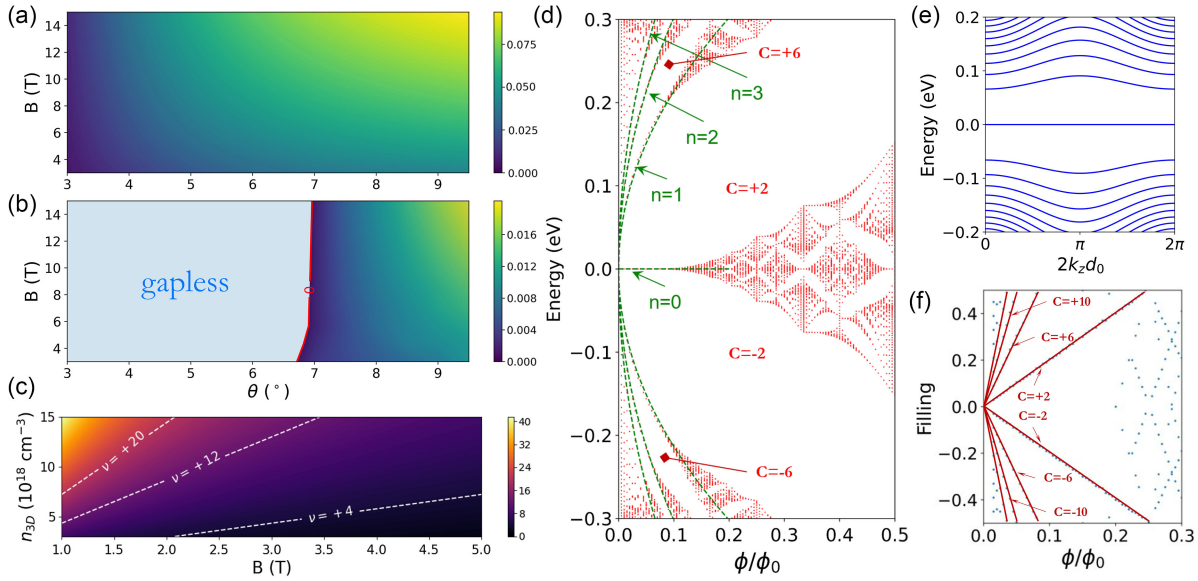

FIG. 3. (a) Global gap (in units of eV) between the first and the zeroth 3D LLs under $B = 3$–15 T for $\theta = 3.0$–$9.5°$. (b) Global gap between the second and the first 3D LLs in the same parameter space as (a). The gap is closed for $\theta \lessapprox 7°$. (c) Color map of the filling factor of 3D LLs in bulk ATG as a function of 3D electron density and magnetic field. The white dashed lines indicates the different integer fillings. (d) Hofstadter butterfly of bulk ATG for $k_z = 0$ and $\theta = 7°$ for one spin sector. Green dashed lines mark the calculated Laudau-level dispersions for $n = 1, 2, 3$ using the approximated Hamiltonian Eq. (3). The Chern number of the gaps are given. (e) k_z dispersions of LLs at $B = 9.8$ T. (f) Wannier plot associated with Hofstadter butterfly in (d).

to exactly dispersionless 3D zeroth LL [see Fig. 3(e)] if the small coordinate-rotation effect is omitted.

The moiré periodicity splits LLs in a fractal manner forming the well-known Hofstadter butterfly [91–93,101–103]. Our calculations [83] show that for $\theta = 7°$, the fractal splitting of the first LL starts at $B \sim 100$ T, which is way beyond the usual experimentally achievable magnitude [see Fig. 2(d)]. Therefore, the renormalized Dirac Hamiltonian Eq. (3) suffices to get the qualitative LL structure of the bulk ATG if $\theta \gtrapprox 6°$. Under $B = 9.8$ T, the first and zeroth LLs of the bulk ATG at $\theta = 7°$, extracted from Hofstadter butterfly calculations, are separated in energy by a large gap ~66 meV; and the first and second LLs are also separated by a global gap ~2 meV [see Fig. 2(e)]. Consequently, several quantized Hall conductivities may be observed. Specifically, when the nth LL is occupied and is separated from the higher one by a global gap, the Hall conductivity should follow the sequence

$$\sigma_{xy} = 2(4n+2)\frac{e^2}{2d_0 h}, \tag{4}$$

where the prefactor of 2 comes from spin degeneracy . This can be shown by the Wannier plot (from one spin species) in Fig. 3(f). According to the Diophantine equation, the slope of each line is precisely the Chern number of the filled Hofstadter bands [104–107]. The eightfold degeneracy is due to two Dirac cones in each of two valleys for two spin sectors. The calculated global gap between the first and zeroth 3D LLs in the (B, θ) parameter space is presented in Fig. 3(a) [see Fig. 3(b) for the gap between second and first 3D Laudau levels], which cearly supports 3D QHE over a wide range of twist angles. The Hofstadter butterfly spectra for $\theta \sim 2°$ show more delicate structures at low energies, which are presented in the Supplemental Material [83].

The exact flatness of the 3D zeroth Landau is protected by a particle-hole symmetry of the Bistritzer-MacDonald type continuum model [5,6,86], which pins the zeroth LL exactly to the Dirac point of the same energy at each k_z. Including the frame-rotation effect would break the particle-hole symmetry that introduces a k_z-dependent energy shift $\sim 2\gamma_0 \cos^2(2k_z d_0)$ [2], with $\gamma_0 = (9u_0'^2 a)/(2\pi\hbar v_F)$. This is the bandwidth (~7 meV) acquired by the 3D zeroth LL, independent of the twist angle. Nevertheless, the k_z dispersion γ_0 is at least an order of magnitude smaller than the LL spacing $\hbar\omega_c$ even under a weak magnetic field $B =$ 1 T ($\hbar\omega_c \sim 30$ meV), which would not affect the 3D QHE discussed above. Unlike the quantum Hall problem in 2D electron gas or in graphene, here the degeneracy of each zeroth LL is $D = 8BSN_z/\phi_0$, where B, S, N_z denote the magnetic field, total cross-sectional area of the bulk system, and number of primitive cells in the out-of-plane direction, respectively. The factor of 8 comes from valley, spin, and orbital degeneracy. The additional k_z degeneracy may lead to a variety of unconventional correlated and topological states for the partially occupied 3D zeroth LL. For example, at partial integer fillings a gap may be opened up due to strong e-e interaction effects, such that the system may undergo a field-induced metal-to-insulator transition

through the spontaneous breaking of flavor (valley and spin) symmetry. The additional k_z degeneracy may lead to further out-of-plane charge modulation driven by *e-e* and/or electron-phonon couplings, which may give rise to potential 3D topological charge density wave state. Other new states of matter are also anticipated at fractional fillings of the 3D zeroth LL. We note that although it is difficult to introduce charge carriers to the bulk ATG system using electrostatic gating methods, the actual ATG sample turns out to be naturally charge doped with carrier density $\sim 10^{19}$ cm^{-3} [108]. Consequently, the Landau-level filling factor can be effectively tuned by increasing magnetic field, so that the proposed 3D quantum Hall physics becomes experimentally feasible.

Discussions.—The physics of bulk ATG has even more to explore than TBG. First, when $\theta < 2\theta_m^{(1)}$, under zero magnetic fields, the flat bands of magic-angle TBG coexist with linearly dispersive Dirac fermions [Fig. 2(c)], and the *e-e* interaction effects and electron-phonon coupling effects of such peculiar band structures are open questions. To answer these questions, we propose to apply gate voltages to BN-encapsulated ATG thin film with thickness of tens of nanometers. For example, when the twist angle $\sim 1°$ and the thickness ~ 20 nm, a straightforward estimation shows that one can completely fill or deplete a moiré band by electrostatic gating with nondisruptive gate voltages, which may unveil potential correlated phenomena at partial filling of the flat bands under zero magnetic field. In the meanwhile, a 20 nm thin film (containing 30 primitive cells) is thick enough to resolve the magic momenta in the system. Second, when $\theta < 2\theta_m^{(2)}$, topological flat bands of TBG at multiple magic angles are integrated into a single bulk ATG system, and unusual interacting ground states would be anticipated. Last, when θ is sufficiently larger than $2\theta_m^{(1)}$, dispersionless 3D zeroth LLs would emerge. Unprecedented quantum states of matter may emerge in the partially occupied dispersionless 3D LLs [109,110], which deserves further explorations.

This work is supported by the National Natural Science Foundation of China (Grants No. 12174257 and No. 12027804), the National Key R&D program of China (Grant No. 2020YFA0309601), the Science and Technology Commission of the Shanghai Municipality (Grant No. 21JC1405100), and the start-up grant of ShanghaiTech University.

*These authors contributed equally to this work.
†wangzhj3@shanghaitech.edu.cn
‡liujp@shanghaitech.edu.cn

[1] R. Bistritzer and A. H. MacDonald, Proc. Natl. Acad. Sci. U.S.A. **108**, 12233 (2011).
[2] J. M. B. Lopes dos Santos, N. M. R. Peres, and A. H. Castro Neto, Phys. Rev. Lett. **99**, 256802 (2007).
[3] S. Shallcross, S. Sharma, E. Kandelaki, and O. A. Pankratov, Phys. Rev. B **81**, 165105 (2010).
[4] G. Tarnopolsky, A. J. Kruchkov, and A. Vishwanath, Phys. Rev. Lett. **122**, 106405 (2019).
[5] J. Liu, J. Liu, and X. Dai, Phys. Rev. B **99**, 155415 (2019).
[6] Z. Song, Z. Wang, W. Shi, G. Li, C. Fang, and B. A. Bernevig, Phys. Rev. Lett. **123**, 036401 (2019).
[7] J. Ahn, S. Park, and B.-J. Yang, Phys. Rev. X **9**, 021013 (2019).
[8] H. C. Po, L. Zou, T. Senthil, and A. Vishwanath, Phys. Rev. B **99**, 195455 (2019).
[9] N. Bultinck, S. Chatterjee, and M. P. Zaletel, Phys. Rev. Lett. **124**, 166601 (2020).
[10] N. Bultinck, E. Khalaf, S. Liu, S. Chatterjee, A. Vishwanath, and M. P. Zaletel, Phys. Rev. X **10**, 031034 (2020).
[11] J. Wang, Y. Zheng, A. J. Millis, and J. Cano, Phys. Rev. Res. **3**, 023155 (2021).
[12] H. Shi and X. Dai, Phys. Rev. B **106**, 245129 (2022).
[13] Y. Cao, V. Fatemi, S. Fang, K. Watanabe, T. Taniguchi, E. Kaxiras, and P. Jarillo-Herrero, Nature (London) **556**, 43 (2018).
[14] M. Yankowitz, S. Chen, H. Polshyn, Y. Zhang, K. Watanabe, T. Taniguchi, D. Graf, A. F. Young, and C. R. Dean, Science **363**, 1059 (2019).
[15] E. Codecido, Q. Wang, R. Koester, S. Che, H. Tian, R. Lv, S. Tran, K. Watanabe, T. Taniguchi, F. Zhang, M. Bockrath, and C. N. Lau, Sci. Adv. **5**, eaaw9770 (2019).
[16] X. Lu, P. Stepanov, W. Yang, M. Xie, M. A. Aamir, I. Das, C. Urgell, K. Watanabe, T. Taniguchi, G. Zhang, A. Bachtold, A. H. MacDonald, and D. K. Efetov, Nature (London) **574**, 653 (2019).
[17] P. Stepanov, I. Das, X. Lu, A. Fahimniya, K. Watanabe, T. Taniguchi, F. H. L. Koppens, J. Lischner, L. Levitov, and D. K. Efetov, Nature (London) **583**, 375 (2020).
[18] Y. Saito, J. Ge, K. Watanabe, T. Taniguchi, and A. F. Young, Nat. Phys. **16**, 926 (2020).
[19] X. Liu, Z. Wang, K. Watanabe, T. Taniguchi, O. Vafek, and J. Li, Science **371**, 1261 (2021).
[20] Y. Cao, D. Rodan-Legrain, J. M. Park, N. F. Yuan, K. Watanabe, T. Taniguchi, R. M. Fernandes, L. Fu, and P. Jarillo-Herrero, Science **372**, 264 (2021).
[21] Y. Cao, V. Fatemi, A. Demir, S. Fang, S. L. Tomarken, J. Y. Luo, J. D. Sanchez-Yamagishi, K. Watanabe, T. Taniguchi, E. Kaxiras *et al.*, Nature (London) **556**, 80 (2018).
[22] A. Kerelsky, L. J. McGilly, D. M. Kennes, L. Xian, M. Yankowitz, S. Chen, K. Watanabe, T. Taniguchi, J. Hone, C. Dean *et al.*, Nature (London) **572**, 95 (2019).
[23] Y. Jiang, X. Lai, K. Watanabe, T. Taniguchi, K. Haule, J. Mao, and E. Y. Andrei, Nature (London) **573**, 91 (2019).
[24] Y. Xie, B. Lian, B. Jäck, X. Liu, C.-L. Chiu, K. Watanabe, T. Taniguchi, B. A. Bernevig, and A. Yazdani, Nature (London) **572**, 101 (2019).
[25] Y. Choi, J. Kemmer, Y. Peng, A. Thomson, H. Arora, R. Polski, Y. Zhang, H. Ren, J. Alicea, G. Refael, F. von Oppen, K. Watanabe, T. Taniguchi, and S. Nadj-Perge, Nat. Phys. **15**, 1174 (2019).

[26] M. Serlin, C. Tschirhart, H. Polshyn, Y. Zhang, J. Zhu, K. Watanabe, T. Taniguchi, L. Balents, and A. Young, Science **367**, 900 (2019).

[27] A. L. Sharpe, E. J. Fox, A. W. Barnard, J. Finney, K. Watanabe, T. Taniguchi, M. A. Kastner, and D. Goldhaber-Gordon, Science **365**, 605 (2019).

[28] L. Balents, C. R. Dean, D. K. Efetov, and A. F. Young, Nat. Phys. **16**, 725 (2020).

[29] E. Y. Andrei, D. K. Efetov, P. Jarillo-Herrero, A. H. MacDonald, K. F. Mak, T. Senthil, E. Tutuc, A. Yazdani, and A. F. Young, Nat. Rev. Mater. **6**, 201 (2021).

[30] J. Liu and X. Dai, Nat. Rev. Phys. **3**, 367 (2021).

[31] P. Stepanov, M. Xie, T. Taniguchi, K. Watanabe, X. Lu, A. H. MacDonald, B. A. Bernevig, and D. K. Efetov, Phys. Rev. Lett. **127**, 197701 (2021).

[32] K. P. Nuckolls, M. Oh, D. Wong, B. Lian, K. Watanabe, T. Taniguchi, B. A. Bernevig, and A. Yazdani, Nature (London) **588**, 610 (2020).

[33] S. Wu, Z. Zhang, K. Watanabe, T. Taniguchi, and E. Y. Andrei, Nat. Mater. **20**, 488 (2021).

[34] I. Das, X. Lu, J. Herzog-Arbeitman, Z.-D. Song, K. Watanabe, T. Taniguchi, B. A. Bernevig, and D. K. Efetov, Nat. Phys. **17**, 710 (2021).

[35] A. T. Pierce, Y. Xie, J. M. Park, E. Khalaf, S. H. Lee, Y. Cao, D. E. Parker, P. R. Forrester, S. Chen, K. Watanabe *et al.*, Nat. Phys. **17**, 1210 (2021).

[36] C. Shen, J. Ying, L. Liu, J. Liu, N. Li, S. Wang, J. Tang, Y. Zhao, Y. Chu, K. Watanabe, T. Taniguchi, R. Yang, D. Shi, F. Qu, L. Lu, W. Yang, and G. Zhang, Chin. Phys. Lett. **38**, 047301 (2021).

[37] J. Kang and O. Vafek, Phys. Rev. Lett. **122**, 246401 (2019).

[38] K. Seo, V. N. Kotov, and B. Uchoa, Phys. Rev. Lett. **122**, 246402 (2019).

[39] M. Xie and A. H. MacDonald, Phys. Rev. Lett. **124**, 097601 (2020).

[40] F. Wu, Phys. Rev. B **99**, 195114 (2019).

[41] F. Wu and S. Das Sarma, Phys. Rev. Lett. **124**, 046403 (2020).

[42] J. Liu and X. Dai, Phys. Rev. B **103**, 035427 (2021).

[43] Y. Zhang, K. Jiang, Z. Wang, and F. Zhang, Phys. Rev. B **102**, 035136 (2020).

[44] K. Hejazi, X. Chen, and L. Balents, Phys. Rev. Res. **3**, 013242 (2021).

[45] J. Kang and O. Vafek, Phys. Rev. B **102**, 035161 (2020).

[46] B.-B. Chen, Y. D. Liao, Z. Chen, O. Vafek, J. Kang, W. Li, and Z. Y. Meng, Nat. Commun. **12**, 5480 (2021).

[47] C. Lu, Y. Zhang, Y. Zhang, M. Zhang, C.-C. Liu, Y. Wang, Z.-C. Gu, W.-Q. Chen, and F. Yang, Phys. Rev. B **106**, 024518 (2022).

[48] Y. Da Liao, J. Kang, C. N. Breiø, X. Y. Xu, H.-Q. Wu, B. M. Andersen, R. M. Fernandes, and Z. Y. Meng, Phys. Rev. X **11**, 011014 (2021).

[49] B. A. Bernevig, Z.-D. Song, N. Regnault, and B. Lian, Phys. Rev. B **103**, 205413 (2021).

[50] B. Lian, Z.-D. Song, N. Regnault, D. K. Efetov, A. Yazdani, and B. A. Bernevig, Phys. Rev. B **103**, 205414 (2021).

[51] F. Xie, A. Cowsik, Z.-D. Song, B. Lian, B. A. Bernevig, and N. Regnault, Phys. Rev. B **103**, 205416 (2021).

[52] T. Soejima, D. E. Parker, N. Bultinck, J. Hauschild, and M. P. Zaletel, Phys. Rev. B **102**, 205111 (2020).

[53] P. Potasz, M. Xie, and A. H. MacDonald, Phys. Rev. Lett. **127**, 147203 (2021).

[54] X. Zhang, G. Pan, Y. Zhang, J. Kang, and Z. Y. Meng, Chin. Phys. Lett. **38**, 077305 (2021).

[55] J. S. Hofmann, E. Khalaf, A. Vishwanath, E. Berg, and J. Y. Lee, Phys. Rev. X **12**, 011061 (2022).

[56] D. E. Parker, T. Soejima, J. Hauschild, M. P. Zaletel, and N. Bultinck, Phys. Rev. Lett. **127**, 027601 (2021).

[57] W.-Y. He, D. Goldhaber-Gordon, and K. T. Law, Nat. Commun. **11**, 1650 (2020).

[58] J. Zhu, J.-J. Su, and A. H. MacDonald, Phys. Rev. Lett. **125**, 227702 (2020).

[59] C. Huang, N. Wei, and A. H. MacDonald, Phys. Rev. Lett. **126**, 056801 (2021).

[60] X. Ying, M. Ye, and L. Balents, Phys. Rev. B **103**, 115436 (2021).

[61] Z.-D. Song and B. A. Bernevig, Phys. Rev. Lett. **129**, 047601 (2022).

[62] C. R. Dean, A. F. Young, I. Meric, C. Lee, L. Wang, S. Sorgenfrei, K. Watanabe, T. Taniguchi, P. Kim, K. L. Shepard *et al.*, Nat. Nanotechnol. **5**, 722 (2010).

[63] C. Liu, Z. Li, R. Qiao, Q. Wang, Z. Zhang, F. Liu, Z. Zhou, N. Shang, H. Fang, M. Wang *et al.*, Nat. Mater. **21**, 1263 (2022).

[64] X. Liu, Z. Hao, E. Khalaf, J. Y. Lee, Y. Ronen, H. Yoo, D. Haei Najafabadi, K. Watanabe, T. Taniguchi, A. Vishwanath, and P. Kim, Nature (London) **583**, 221 (2020).

[65] Y. Cao, D. Rodan-Legrain, O. Rubies-Bigorda, J. M. Park, K. Watanabe, T. Taniguchi, and P. Jarillo-Herrero, Nature (London) **583**, 215 (2020).

[66] C. Shen, Y. Chu, Q. Wu, N. Li, S. Wang, Y. Zhao, J. Tang, J. Liu, J. Tian, K. Watanabe, T. Taniguchi, R. Yang, Z. Y. Meng, D. Shi, O. V. Yazyev, and G. Zhang, Nat. Phys. **16**, 520 (2020).

[67] J. Liu, Z. Ma, J. Gao, and X. Dai, Phys. Rev. X **9**, 031021 (2019).

[68] M. Koshino, Phys. Rev. B **99**, 235406 (2019).

[69] J. Y. Lee, E. Khalaf, S. Liu, X. Liu, Z. Hao, P. Kim, and A. Vishwanath, Nat. Commun. **10**, 5333 (2019).

[70] P. J. Ledwith, A. Vishwanath, and E. Khalaf, Phys. Rev. Lett. **128**, 176404 (2022).

[71] J. Wang and Z. Liu, Phys. Rev. Lett. **128**, 176403 (2022).

[72] S. Zhang, B. Xie, Q. Wu, J. Liu, and O. V. Yazyev, Nano Lett. **23**, 2921 (2023).

[73] E. Khalaf, A. J. Kruchkov, G. Tarnopolsky, and A. Vishwanath, Phys. Rev. B **100**, 085109 (2019).

[74] B. Xie, R. Peng, S. Zhang, and J. Liu, npj Comput. Mater. **8**, 110 (2022).

[75] P. J. Ledwith, E. Khalaf, Z. Zhu, S. Carr, E. Kaxiras, and A. Vishwanath, arXiv:2111.11060.

[76] N. Leconte, Y. Park, J. An, A. Samudrala, and J. Jung, 2D Mater. **9**, 044002 (2022).

[77] T. Cea, N. R. Walet, and F. Guinea, Nano Lett. **19**, 8683 (2019).

[78] Y. Cao, J. M. Park, K. Watanabe, T. Taniguchi, and P. Jarillo-Herrero, Nature (London) **595**, 526 (2021).

[79] Z. Hao, A. M. Zimmerman, P. Ledwith, E. Khalaf, D. H. Najafabadi, K. Watanabe, T. Taniguchi, A. Vishwanath, and P. Kim, Science **371**, 1133 (2021).
[80] H. Polshyn, J. Zhu, M. Kumar, Y. Zhang, F. Yang, C. Tschirhart, M. Serlin, K. Watanabe, T. Taniguchi, A. MacDonald *et al.*, Nature (London) **588**, 66 (2020).
[81] Q. Li, B. Cheng, M. Chen, B. Xie, Y. Xie, P. Wang, F. Chen, Z. Liu, K. Watanabe, T. Taniguchi, S.-J. Liang, D. Wang, C. Wang, Q.-H. Wang, J. Liu, and F. Miao, Nature (London) **609**, 479 (2022).
[82] Z.-J. Wang, X. Kong, Y. Huang, J. Li, L. Bao, K. Cao, Y. Hu, J. Cai, L. Wang, H. Chen, Y. Wu, Y. Zhang, F. Pang, Z. Cheng, P. Babor, M. Kolibal, Z. Liu, Y. Chen, Q. Zhang, Y. Cui, K. Liu, H. Yang, X. Bao, H.-J. Gao, Z. Liu, W. Ji, F. Ding, and M.-G. Willinger, Nat. Mater., 10.1038/s41563-023-01632-y (2023).
[83] See Supplemental Material at http://link.aps.org/supplemental/10.1103/PhysRevLett.132.056601 for (a) a cross-sectional STEM image of the twisted graphene spiral sample, (b) details of the continuum model for bulk alternating twisted graphite (including Refs. [1,2,84,85]), (c) detailed band structures and topological transitions in bulk alternating twisted graphite (including Refs. [86]), (d) lattice relaxations and atomistic tight-binding model for bulk alternating twisted graphite (including Refs. [87–90]), (e) detailed formalism of calculating Hofstadter butterfly spectra based on the continuum model, (f) more results about the Hofstadter butterfly spectra (including Refs. [91–95]), (g) bound states associated with the spiral dislocation line (including Refs. [87,88]), and (h) results of surface-state calculations for the ATG system (including Ref. [96]).
[84] P. Moon and M. Koshino, Phys. Rev. B **87**, 205404 (2013).
[85] M. Koshino, N. F. Q. Yuan, T. Koretsune, M. Ochi, K. Kuroki, and L. Fu, Phys. Rev. X **8**, 031087 (2018).
[86] K. Hejazi, C. Liu, H. Shapourian, X. Chen, and L. Balents, Phys. Rev. B **99**, 035111 (2019).
[87] A. P. Thompson, H. M. Aktulga, R. Berger, D. S. Bolintineanu, W. M. Brown, P. S. Crozier, P. J. in 't Veld, A. Kohlmeyer, S. G. Moore, T. D. Nguyen, R. Shan, M. J. Stevens, J. Tranchida, C. Trott, and S. J. Plimpton, Comput. Phys. Commun. **271**, 108171 (2022).
[88] J. H. Los and A. Fasolino, Phys. Rev. B **68**, 024107 (2003).
[89] N. N. T. Nam and M. Koshino, Phys. Rev. B **96**, 075311 (2017).
[90] M. Angeli, D. Mandelli, A. Valli, A. Amaricci, M. Capone, E. Tosatti, and M. Fabrizio, Phys. Rev. B **98**, 235137 (2018).
[91] R. Bistritzer and A. H. MacDonald, Phys. Rev. B **84**, 035440 (2011).
[92] K. Hejazi, C. Liu, and L. Balents, Phys. Rev. B **100**, 035115 (2019).
[93] Y.-H. Zhang, H. C. Po, and T. Senthil, Phys. Rev. B **100**, 125104 (2019).
[94] K. E. Cahill and R. J. Glauber, Phys. Rev. **177**, 1857 (1969).
[95] P. Streda, J. Phys. C **15**, L717 (1982).
[96] M. L. Sancho, J. L. Sancho, J. L. Sancho, and J. Rubio, J. Phys. F **15**, 851 (1985).
[97] J. M. B. Lopes dos Santos, N. M. R. Peres, and A. H. Castro Neto, Phys. Rev. B **86**, 155449 (2012).
[98] B. A. Bernevig, T. L. Hughes, S. Raghu, and D. P. Arovas, Phys. Rev. Lett. **99**, 146804 (2007).
[99] F. Tang, Y. Ren, P. Wang, R. Zhong, J. Schneeloch, S. A. Yang, K. Yang, P. A. Lee, G. Gu, Z. Qiao *et al.*, Nature (London) **569**, 537 (2019).
[100] K. Novoselov, A. K. Geim, S. Morozov, D. Jiang, M. Katsnelson, I. Grigorieva, S. Dubonos, and A. Firsov, Nature (London) **438**, 197 (2005).
[101] R. de Gail, M. O. Goerbig, F. Guinea, G. Montambaux, and A. H. Castro Neto, Phys. Rev. B **84**, 045436 (2011).
[102] B. Lian, F. Xie, and B. A. Bernevig, Phys. Rev. B **102**, 041402(R) (2020).
[103] X. Wang and O. Vafek, Phys. Rev. B **106**, L121111 (2022).
[104] D. Xiao, M.-C. Chang, and Q. Niu, Rev. Mod. Phys. **82**, 1959 (2010).
[105] D. J. Thouless, M. Kohmoto, M. P. Nightingale, and M. den Nijs, Phys. Rev. Lett. **49**, 405 (1982).
[106] M. Kohmoto, Phys. Rev. B **39**, 11943 (1989).
[107] I. Dana, Y. Avron, and J. Zak, J. Phys. C **18**, L679 (1985).
[108] Y. Zhang, B. Xie, Y. Yang, Y. Wu, X. Lu, Y. Hu, Y. Ding, J. He, P. Dong, J. Wang, X. Zhou, J. Liu, Z.-J. Wang, and J. Li, arXiv:2311.15319.
[109] X. Qiu, R. Joynt, and A. H. MacDonald, Phys. Rev. B **42**, 1339 (1990).
[110] J. D. Naud, L. P. Pryadko, and S. L. Sondhi, Phys. Rev. Lett. **85**, 5408 (2000).